Received: 17 July 2020 | Revised: 12 October 2020 | Accepted: 13 October 2020

DOI: 10.1002/cm.21637

SHORT REPORT

WILEY

Cilium axoneme internalization and degradation in chytrid fungi

Claire M Venard[1] | Krishna Kumar Vasudevan[1] | Tim Stearns[1,2]

[1]Department of Biology, Stanford University, Stanford, California

[2]Department of Genetics, Stanford University, Stanford, California

Correspondence
Tim Stearns, Department of Biology, Stanford University, Stanford, CA.
Email: stearns@stanford.edu

Funding information
National Center for Research Resources, Grant/Award Number: 1S10RR026780-01; National Human Genome Research Institute, Grant/Award Number: 5T32HG000044-23; National Institute of General Medical Sciences, Grant/Award Number: 1R35GM130286

Abstract

Loss of the cilium is important for cell cycle progression and certain developmental transitions. Chytrid fungi are a group of basal fungi that have retained centrioles and cilia, and they can disassemble their cilia via axoneme internalization as part of the transition from free-swimming spores to sessile sporangia. While this type of cilium disassembly has been observed in many single-celled eukaryotes, it has not been well characterized because it is not observed in common model organisms. To better characterize cilium disassembly via axoneme internalization, we focused on chytrids *Rhizoclosmatium globosum* and *Spizellomyces punctatus* to represent two lineages of chytrids with different motility characteristics. Our results show that each chytrid species can reel in its axoneme into the cell body along its cortex on the order of minutes, while *S. punctatus* has additional faster ciliary compartment loss and lash-around mechanisms. *S. punctatus* retraction can also occur away from the cell cortex and is partially actin dependent. Post-internalization, the tubulin of the axoneme is degraded in both chytrids over the course of about 2 hr. Axoneme disassembly and axonemal tubulin degradation are both partially proteasome dependent. Overall, chytrid cilium disassembly is a fast process that separates axoneme internalization and degradation.

KEYWORDS

axoneme, Chytridiomycota, cilia, proteolysis, RRID:AB_2535778, RRID:AB_2535809, RRID:AB_2650560, RRID:AB_2715541, RRID:AB_477583, RRID:AB_609894, RRID:AB_621847, RRID:AB_621848, RRID:SCR_000432, RRID:SCR_002285, RRID:SCR_003070, RRID:SCR_016865, tubulin

1 | INTRODUCTION

The eukaryotic motile cilium, also known as a flagellum in many single-celled organisms, is a compartment that extends from the plasma membrane and is built on a complex microtubule structure called the axoneme. The axoneme has a characteristic 9 + 2 structure, with nine symmetric doublet microtubules surrounding two singlet microtubules in the center (Linck, Chemes, & Albertini, 2016). Each cilium has a centriole at its base, often referred to as a basal body. For most eukaryotes, cilium disassembly is necessary for centrioles to be released from the axoneme and plasma membrane so that they can take part in the mitotic spindle and be segregated to daughter cells (Liang, Meng, Zhu, & Pan, 2016). Cilium disassembly is also required for developmental transitions of some single-celled eukaryotes. One example is *Naegleria gruberi*, which loses its cilium in the transition from a free-swimming state to an amoeboid, mitotic state (Fulton, 1977). Therefore, cilium disassembly is important for both entering mitosis in most eukaryotes and developmental transitions for some single-celled eukaryotes.

Multiple mechanisms of cilium loss occur in eukaryotes, with most studies coming from analyzing only a few model systems, such as cultured mammalian cells and the green alga *Chlamydomonas reinhardtii*.

Two mechanisms are observed in both of these very different organisms: (a) rapid severing of the cilium at its base (Lohret, McNally, & Quarmby, 1998; Mirvis, Siemers, Nelson, & Stearns, 2019) and (b) gradual (over hours) shortening of the cilium (Mirvis et al., 2019; Piao et al., 2009). However, some organisms undergo a different mechanism of cilium disassembly that involves internalization of an intact ciliary axoneme. Bloodgood (1974) reported axoneme internalization as at least one mechanism of cilium disassembly in 56/67 species of algae, fungi, and other single-celled eukaryotes examined. This mechanism has not been observed in mammalian cells or *Chlamydomonas* but does bear similarities to other events that result in internalization of an axoneme, such as animal fertilization (Bedford, 1972; Simerly et al., 1995).

We chose to study cilium disassembly via axoneme internalization in chytrid fungi. Chytrids are a group of basal fungi that have retained centrioles and cilia, which have been lost in higher fungi (James et al., 2006; James et al., 2006). Although chytrids are a large, diverse group, a stereotypical chytrid life cycle starts with a free-swimming zoospore with a posterior cilium; zoospores are typically a few microns in diameter with cilia 10s of microns long. Cilium disassembly occurs during the zoospore-sporangium transition, as cells form sessile sporangia with a chitin-based cell wall and actin-based rhizoids. These sporangia grow in size with accompanying nuclear divisions, followed by formation of zoospores and their release (Berger, Hyatt, Speare, & Longcore, 2005; Medina et al., 2020; Sparrow, 1960).

Chytrids are a useful organism to study this process for several reasons. First, general interest in chytrids has risen steeply since the discovery of the chytrid *Batrachochytrium dendrobatidis* as the causative agent of chytridiomycosis, a disease contributing to worldwide amphibian die-off (James et al., 2015; Longcore, Pessier, & Nichols, 1999; Pessier, Nichols, Longcore, & Fuller, 1999). Second, several different types of axoneme internalization have been previously identified in chytrids via live microscopy, and confirmation that the axoneme is internalized has been shown via transmission electron microscopy (TEM) (Chong & Barr, 1973; Koch, 1968). This behavior has also been referenced in more recent work (Fritz-Laylin, Lord, & Mullins, 2017; Leshem, Letcher, Powell, & Sukenik, 2016; Medina et al., 2020; Vélez, Letcher, Schultz, Powell, & Churchill, 2011), setting the stage for a more comprehensive understanding of chytrid axoneme internalization and the fate of internalized axonemes.

We selected two different chytrids for our experiments, *Rhizoclosmatium globosum* and *Spizellomyces punctatus*. Within the chytrid lineage, some species rely solely on cilia for movement while others have the additional ability to crawl via amoeboid motility (Fritz-Laylin et al., 2017). While *S. punctatus* is an amoeboid chytrid (Medina et al., 2020), *R. globosum* has never been shown to have this ability to crawl (Barr & Hartmann, 1976; Laundon, Chrismas, Wheeler, & Cunliffe, 2020; Letcher et al., 2017; Sparrow, 1960). This difference allowed us to assay whether the more dynamic membrane of amoeboid *S. punctatus* influences its modes of cilium disassembly. In the course of this work we optimized several experimental techniques for use in these chytrids, including live cell imaging, immunofluorescence microscopy, TEM, lysate preparation for western blots, and small molecule inhibitor perturbations. We identify several mechanisms of cilium retraction and show that the tubulin of the internalized axoneme is degraded over time. Overall, chytrid cilium disassembly is a relatively rapid process that consists of distinct phases of axoneme internalization and degradation.

2 | RESULTS AND DISCUSSION

2.1 | Characterizing cilium disassembly mechanisms in *R. globosum* and *S. punctatus*

We first examined the cilium disassembly mechanisms that occur in *R. globosum* and *S. punctatus*, using the nomenclature of Koch (1968) where our observations corresponded to his comprehensive review of retraction in 42 different species of chytrids. To generate populations of zoospores primed for cilium retraction, we grew cells on 1% agar plates with PmTG medium for *R. globosum* and K1 medium for *S. punctatus* (Barr, 1986; Koch, 1957). Overlaying liquid medium on plates with mature sporangia resulted in zoospore release, and plating these zoospores on agar resulted in cilium disassembly in ~60% of zoospores within 10 min.

Imaging live zoospores on agar pads by phase microscopy, we observed several mechanisms of cilium disassembly. For *R. globosum*, in some zoospores the cilium was severed from the cell body (Figure 1a; Video S1). This was described by Koch as flagellar detachment (Koch, 1968) and has also been observed in model systems including *Chlamydomonas* and mammalian cell lines (Lohret et al., 1998; Mirvis et al., 2019). Second, *R. globosum* zoospores retracted their cilia into the cell within a few minutes, visible as gradual shortening of the cilium (Figure 1b; Video S2). Cortical rotation was often seen concurrent with cilium shortening, visible by the rotation of phase-bright objects within the cell as the exterior cilium shortened (Figure 1b; Video S2). Koch referred to these axoneme internalization events with cortical rotation as body-twist retractions and events without cortical rotation as straight-in retractions (Koch, 1968). Because treatment of the axoneme is similar for these two mechanisms, we group them together and term them reeling in retraction.

S. punctatus cells were observed to have these two behaviors (Figure 1c,d; Videos S3 and S4) in addition to several others. In some cases, the cilium wrapped around the outside of the cell, and the ciliary membrane appeared to rapidly merge with the plasma membrane (Figure 1e; Video S5). Koch referred to this mode of axoneme internalization as lash-around retraction, and we use the same term (Koch, 1968). In some conditions, including plating of cells on 120 kPa fibronectin-coated hydrogels, this form of retraction occurred in less than a second (Video S6), similar to that observed for the amoeboid chytrid *B. dendrobatidis* (Fritz-Laylin et al., 2017). In a second type of *S. punctatus*-specific event, the base of the ciliary membrane expanded such that the ciliary compartment merged with the plasma membrane (Figure 1f; Video S7). We term this mode of axoneme internalization, not described by Koch, as ciliary compartment loss retraction.

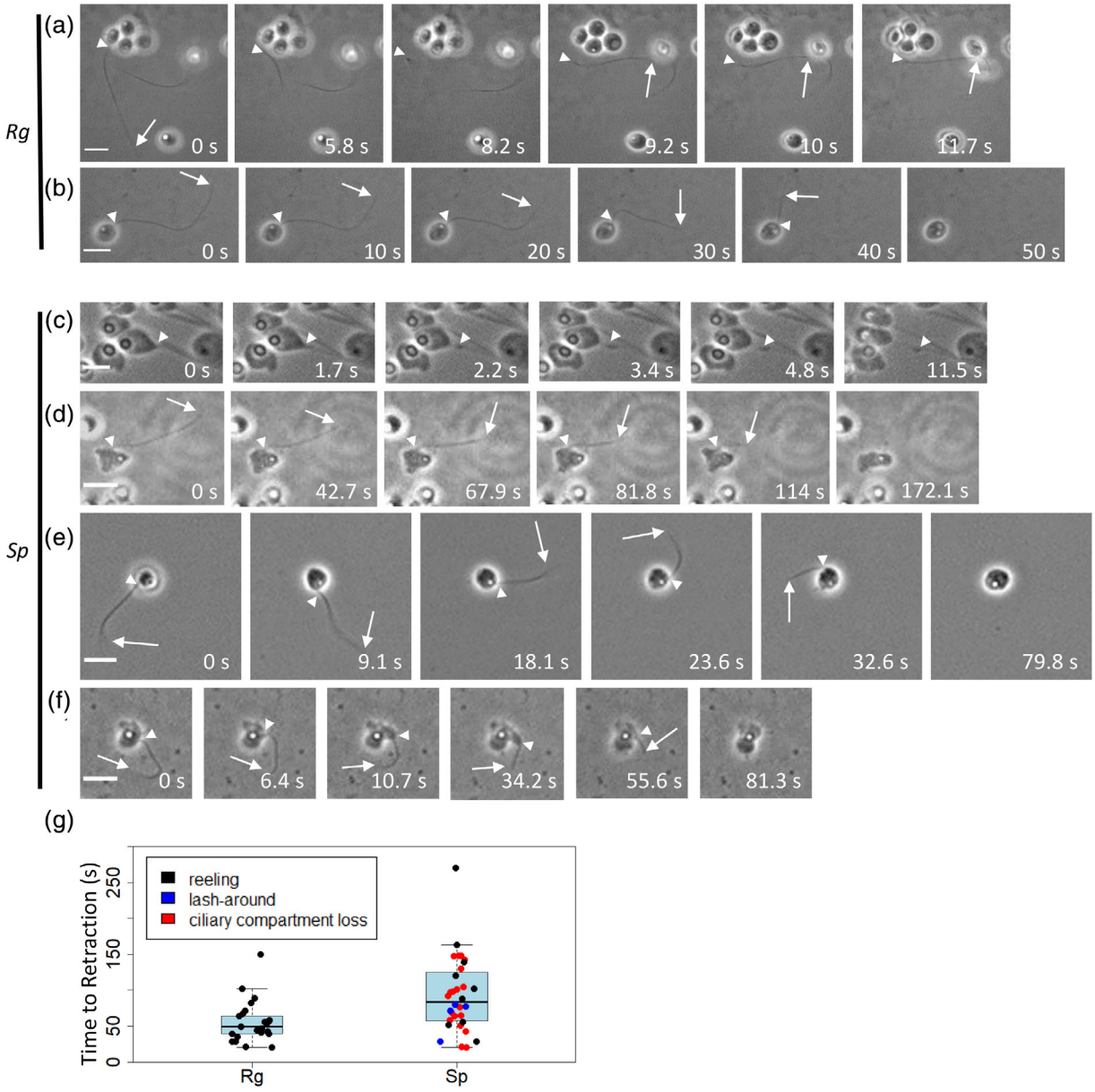

FIGURE 1 Characterizing cilium disassembly mechanisms in *R. globosum* and *S. punctatus*. *R. globosum* and *S. punctatus* zoospores were concentrated and placed between an agar pad and glass coverslip for live cell imaging. Still images were taken from individual movies for each species. (a) Severing and (b) reeling in retraction occurred for *R. globosum*. (c) Severing, (d) reeling in, (e) lash-around, and (f) ciliary compartment loss mechanisms were observed in *S. punctatus*. (g) Box plots with each individual retraction event show the distribution of time to retraction for both *R. globosum* (n = 23 cells) and *S. punctatus* (n = 32 cells). Black dots indicate reeling in retraction (*R. globosum*, n = 23 cells; *S. punctatus*, n = 9 cells), red dots indicate ciliary compartment loss retraction (*S. punctatus*, n = 19 cells), and blue dots indicate lash-around retraction (*S. punctatus*, n = 4 cells). White arrow heads indicate proximal ends of cilia, and white arrows indicate distal ends of cilia. All scale bars are 5 μm [Color figure can be viewed at wileyonlinelibrary.com]

Under standard growth conditions for both species, we did not observe the most common mechanism described by Koch, vesicular retraction, in which the axoneme loops to create a bulge within the ciliary membrane before being fully internalized (Koch, 1968). However, we note that we did observe instances of this axoneme looping under conditions we interpret as being stressful for the cells, such as prolonged observation under a cover slip or high concentrations of DMSO used as vehicle for drug treatments.

To our knowledge, no specific retraction behaviors have been described in previous characterizations of *R. globosum* for comparison (Barr & Hartmann, 1976; Laundon et al., 2020; Letcher et al., 2017; Sparrow, 1960). However, *S. punctatus* has been described with lash-around and vesicular retraction (Koch, 1968; Medina et al., 2020), which is consistent with what we have observed.

To further characterize retraction by species and mechanism, we measured time to retraction, initial cilium length, and cell body

diameter from video sequences of retraction events. On average, *S. punctatus* retraction took longer than *R. globosum* retraction and had a much larger variance (Figure 1g; Table 1). *R. globosum* also had a longer mean initial cilium length and higher rate of retraction compared to *S. punctatus* (Table 1). When the observed retraction mechanisms of *S. punctatus* are considered separately, on average lash-around retraction events were fastest while reeling in retraction events were slowest (Table 2).

2.2 | Characterizing axoneme localization post-retraction in *R. globosum* and *S. punctatus*

We next used a combination of immunofluorescence microscopy and TEM to characterize how the axoneme is internalized. For immunofluorescence visualization of the axoneme, zoospores were fixed before and after retraction induced by plating on agar medium. Antibodies against acetylated tubulin and α-tubulin both stained the cilia of *R. globosum* and *S. punctatus* zoospores (Figure 2a,b; Figure S1). In *R. globosum* cells in the earliest stages of retraction, the internalized axoneme remained close to the cell cortex, suggesting that the axoneme is tethered to the cortex, either as part of the mechanism of internalization or coincident with it (Figure 2c). However, initial stages of retraction in *S. punctatus* did not always occur close to the cortex (Figure 2d,e). In cells with complete cilium retraction before fixation, both chytrids had internalized axonemes that were hoop-shaped, wrapped fully around the cell and consistent with continued axoneme association with the cortex (Figure 2f,g). However, some *S. punctatus* retraction events resulted in an axoneme internalized freely within the cell body, often curled up on itself, pretzel-like (Figure 2h). Both species also had cells with no acetylated tubulin signal and seemingly no internalized axoneme, which presumably corresponded to severing events (Figure 2i,j).

Only a few examples of chytrid axoneme internalization have been observed previously via TEM, and based on these the axoneme is thought to be retracted intact (Chong & Barr, 1973; Koch, 1968). We performed TEM for *R. globosum* and *S. punctatus* after plating zoospores on agar to induce cilium retraction. Consistent with our immunofluorescence observations, the retracted ciliary axonemes for both chytrids were observed near the cortex over an extended length in longitudinal sections (Figure 2k,l, top). In cross-sections, we observed that two axonemes could be found next to each other (Figure 2k,l, bottom). These axonemes showed the canonical 9 + 2 architecture of motile cilia, indicating that axonemes remain intact during internalization, and their paired nature is consistent with the expectation that an axoneme would wrap around the cell one to two times given cilium length and cell diameter (Table 1). The cross-sections also showed that the ciliary axoneme was exposed to the cytoplasm without a surrounding ciliary membrane. Retracted axonemes were also observed away from the plasma membrane for *S. punctatus* (Figure 2m), which is consistent with our immunofluorescence observation that some *S. punctatus* axonemes were found away from the cortex post-retraction.

TABLE 1 *Rhizoclosmatium globosum* and *Spizellomyces punctatus* retraction: parameter quantification

	R. globosum	*S. punctatus*
Time to retraction (s)	55.53 ± 28.12	92.21 ± 51.8
Cilium length (μm)	22.51 ± 3.65	13.87 ± 2.95
Rate of retraction (μm/s)	0.48 ± 0.17	0.22 ± 0.19
Cell diameter (μm)	3.53 ± 0.38	3.81 ± 0.9
Cilium length/cell circumference	2.05 ± 0.35	1.19 ± 0.27

Note: Using the movies referred to in Figure 1 (*R. globosum*, *n* = 23; *S. punctatus*, *n* = 32), time to retraction, cilium length, and cell diameter were measured in ImageJ and used to calculate rate of retraction and number of circumferences of axoneme (cilium length/cell circumference) for individual cells. The reported values for rate of retraction and cilium length/cell circumference are the means of these individual calculations. Values are shown as mean ± *SD*.

2.3 | *S. punctatus* cilium retraction is partially actin dependent

Because *R. globosum* and *S. punctatus* differ dramatically in their membrane dynamics as zoospores, we examined whether the actin-based dynamicity that underlies amoeboid motility in *S. punctatus* influences its retraction behaviors. To test this, we first characterized the actin network of both species. Rhodamine-phalloidin staining of zoospores exposed to an agar substrate revealed that *S. punctatus* had a much

TABLE 2 *Spizellomyces punctatus* retraction: parameter quantification by retraction type

	Reeling in	Ciliary compartment loss	Lash-around
Time to retraction (s)	113.07 ± 73.22	88.21 ± 41.65	64.27 ± 23.97
Cilium length (μm)	13.45 ± 1.73	13.48 ± 3.05	16.67 ± 3.75
Rate of retraction (μm/s)	0.18 ± 0.14	0.22 ± 0.19	0.33 ± 0.25
Cell diameter (μm)	3.74 ± 0.99	3.66 ± 0.83	4.68 ± 0.66
Cilium length/cell circumference	1.18 ± 0.22	1.21 ± 0.30	1.14 ± 0.24

Note: Using the movies referred to in Figure 1 (reeling in, *n* = 9; ciliary compartment loss, *n* = 19; lash-around, *n* = 4), time to retraction, cilium length, and cell diameter were measured in ImageJ to calculate rate of retraction and number of circumferences of axoneme (cilium length/cell circumference) for individual cells. The reported values for rate of retraction and cilium length/cell circumference are the means of these individual calculations. Values are shown as mean ± *SD*.

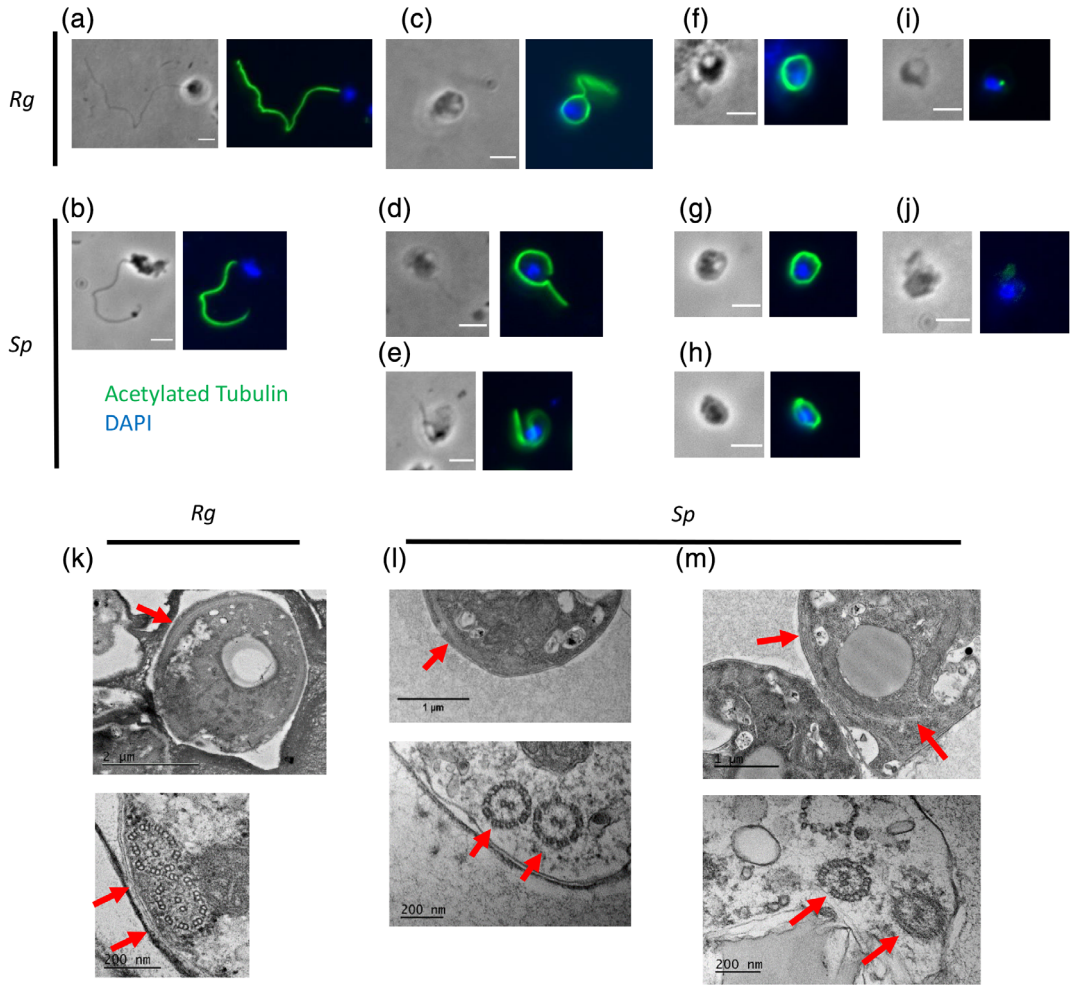

FIGURE 2 Characterizing axoneme localization post-retraction in *R. globosum* and *S. punctatus*. Zoospores were fixed and stained for acetylated tubulin (green) and DNA (blue) for (a) *R. globosum* and (b) *S. punctatus*. After zoospores were plated for 10 min, fixed, and stained, partial retractions at the cortex were seen for (c) *R. globosum* and (d) *S. punctatus*. (e) A partial retraction with axoneme not associated with the cortex was only seen for *S. punctatus*. Hoop shaped axonemes were observed for (f) *R. globosum* and (g) *S. punctatus*. (h) Off-cortex retraction was also seen in *S. punctatus*. Cells without acetylated tubulin staining for (i) *R. globosum* and (j) *S. punctatus* were also observed. TEM 10 min post-retraction show intact axonemes at the cortex for (k) *R. globosum* and (l) *S. punctatus*. Off-cortex axonemes were only observed in (m) *S. punctatus*. (k–m) Axonemes are shown longitudinally (top) and in cross-section (bottom). Red arrows indicate axonemes. Unlabeled scale bars are 3 µm [Color figure can be viewed at wileyonlinelibrary.com]

more extensive actin network, while *R. globosum* had mostly actin patches and was never observed to have a ruffled membrane (Figure 3a-b). This is consistent with actin-filled pseudopods previously observed in *S. punctatus* as well as the amoeboid chytrid *B. dendrobatidis* (Fritz-Laylin et al., 2017; Medina et al., 2020). 1.2 µM latrunculin A disrupted the actin networks in both species, but a vehicle control did not (Figure 3c-h), with cells remaining viable after a 10 min incubation. This concentration of latrunculin A also blocked *S. punctatus*'s ability to crawl, but a vehicle control did not (Videos S8 and S9).

To test whether actin polymerization is required for cilium retraction events, we treated both *R. globosum* and *S. punctatus* with latrunculin A or vehicle control and assessed retraction. After 10 min of latrunculin A treatment, retraction was significantly decreased and remaining ciliated cells significantly increased only in *S. punctatus* cells (Figure 3i,j). Thus, cilium retraction is partially actin dependent in *S. punctatus* but not in *R. globosum*.

We hypothesized that this partial reduction was due to blocking the *S. punctatus*-specific membrane-mediated lash-around and ciliary compartment loss mechanisms while allowing the reeling in retraction that also occurs in *R. globosum*. To test this hypothesis, we observed *S. punctatus* retraction events live via phase microscopy in latrunculin A or vehicle control. The quantification of these movies only included cells that underwent a complete retraction during a movie; all other cells were excluded from the analysis, including cells that retained their cilia. This was done to be able to quantify whether the cells that could retract under latrunculin A treatment did so differently than the control in terms of retraction types or rates of retraction. Overall, some *S. punctatus* zoospores were able to retract their cells in the

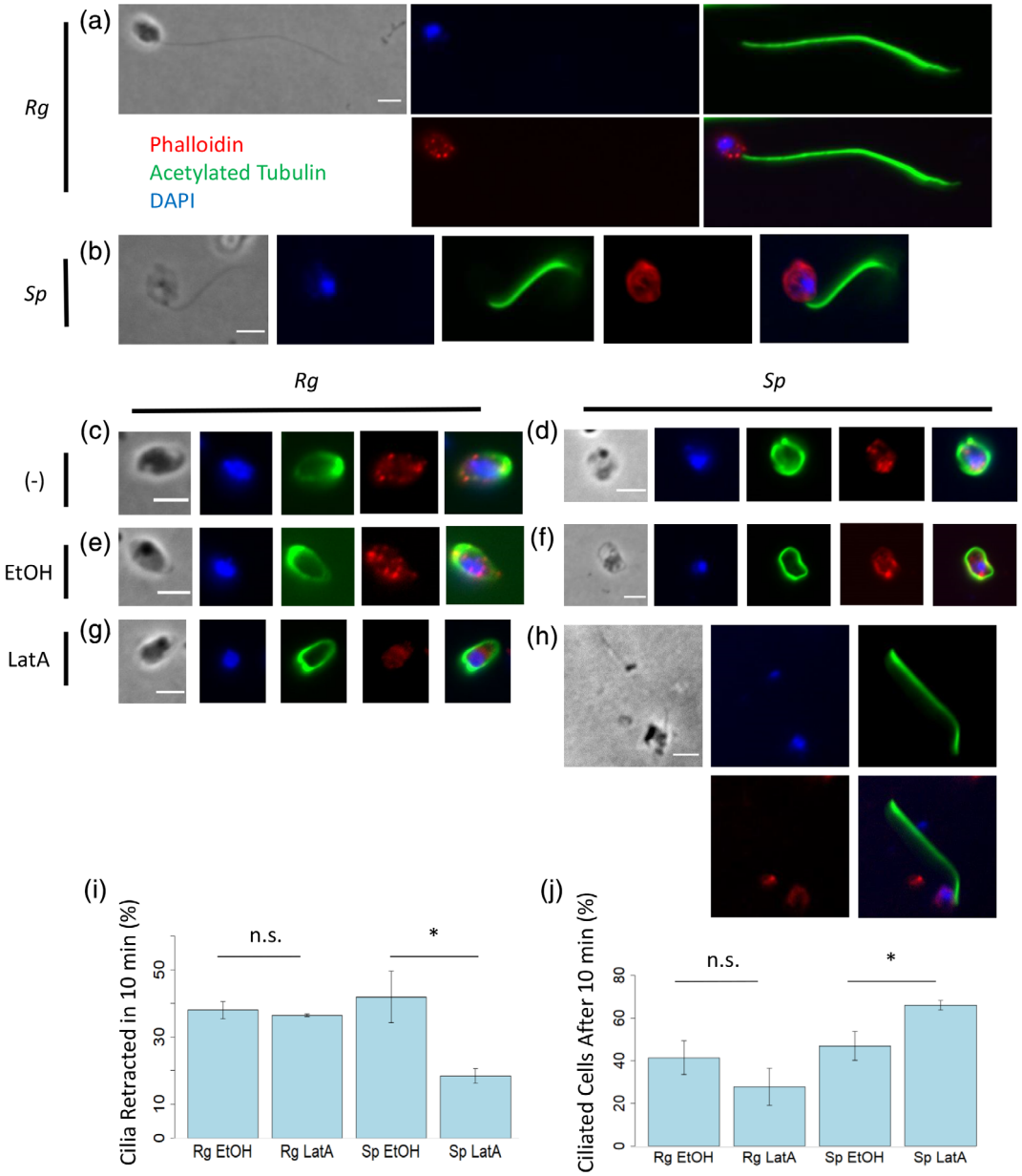

FIGURE 3 *S. punctatus* cilium retraction is partially actin dependent. Cells were fixed and stained for (a) *R. globosum* and (b) *S. punctatus* zoospores. (c) *R. globosum* and (d) *S. punctatus* zoospores were plated for 10 min with no treatment, fixed, and stained. (e) *R. globosum* and (f) *S. punctatus* zoospores were plated for 10 min with 0.5% ethanol, fixed, and stained. (g) *R. globosum* and (h) *S. punctatus* zoospores were plated for 10 min with 1.2 μM latrunculin A, fixed, and stained. All staining is acetylated tubulin (green), rhodamine-phalloidin (red), and DNA (blue). (i) Quantification of the percent of cells with a retracted axoneme after 10 min are shown for *R. globosum* and *S. punctatus* under ethanol (EtOH) and latrunculin A (LatA) treatment (*R. globosum* $p = .586$; *S. punctatus* $p = .02673$). (j) Quantification of the percent of cells with a remaining exterior cilium after 10 min are shown for *R. globosum* and *S. punctatus* under ethanol (EtOH) and latrunculin A (LatA) treatment (*R. globosum* $p = .2909$; *S. punctatus* $p = .03787$). The quantifications are for four independent experiments for *R. globosum* and six for *S. punctatus*. Each condition per experiment quantified 162–757 cells for *R. globosum* and 53–202 cells for *S. punctatus*. Error bars are SEM. * indicates $p < .05$, and n.s. indicates no significant difference. Scale bars are 3 μm [Color figure can be viewed at wileyonlinelibrary.com]

presence of latrunculin A (Table 3; Figure S2). Zoospores that were able to retract did so with a similar distribution of mechanisms as the vehicle control; rates of retraction for each mechanism were also similar, although latrunculin A-treated cells had increased variance compared to the vehicle control (Table 4). These combined results from fixed and live imaging indicate that actin inhibition in *S. punctatus* primarily blocks retraction initiation rather than specific retraction mechanisms.

A possible caveat is that latrunculin A-treated *S. punctatus* cells did have some cortical membrane activity and particle movement

within cells despite not being able to crawl (Video S9), which could indicate some residual actin activity and explain the partial penetrance of the latrunculin A phenotype. Further experiments will be required to determine whether the eventual fate of latrunculin A-treated zoospores that retain their cilia is to undergo delayed retraction or if retraction is completely blocked and prevents life cycle progression.

2.4 | Axonemal tubulin is degraded after internalization

We next investigated the fate of the internalized ciliary axonemes. In the related ciliated fungus *Blastocladiella emersonii* that also undergoes cilium retraction, the internalized axoneme was absent by the time of rhizoid initiation (Truesdell & Cantino, 1971), suggesting that loss of the internalized axoneme occurs in early sporangia. We examined the persistence of the axoneme over time after internalization by immunofluorescence microscopy. At 10 min post-retraction, many cells of both chytrids had hoop-shaped internalized axonemes, with *S. punctatus* also having many pretzel-like retraction events. The "empty" category at 10 min is presumably indicative of the background of cilium severing events, which were more frequent in *R. globosum* in these experiments. In both species, the "empty" category increased over time such that by 2 hr post-retraction, most cells lacked any visible internal axoneme (Figure 4a,b).

We occasionally observed partial axoneme structures that might represent intermediates of axoneme loss (Figure 4a,b). First, for *R. globosum*, we observed cells containing arcs of axoneme that presumably represent partial hoops and could be indicative of axoneme depolymerization from one or both ends (Figure 4c). Plus-end microtubule depolymerizing kinesins are involved in axoneme shortening in *Chlamydomonas* and mammalian cell lines, and their action would be consistent with this observation (Hu, Liang, He, & Pan, 2015; Kim, Lee, Choi, Ringstad, & Dynlacht, 2015; Miyamoto et al., 2015; Piao et al., 2009). Second, we observed cells containing discrete pieces of acetylated tubulin signal consistent with axoneme severing events (Figure 4d). Severing of axonemes via katanin has also been implicated in mammalian and *Chlamydomonas* cilium disassembly (Lohret et al., 1998; Mirvis et al., 2019; Parker et al., 2010). These types of intermediates were also observed for *S. punctatus* (Figure 4e,f).

Intracellular disassembly of the ciliary axoneme would be expected to free a large amount of tubulin heterodimer. To determine the fate of the internalized tubulin, we used western blotting to determine the amount of tubulin in cells at 0 min, 10 min, 1 hr, and 2 hr after plating. Surprisingly, levels of α-tubulin, acetylated tubulin, and β-tubulin decreased relative to total protein over the course of 2 hr at approximately the same rate, whereas histone H3 levels did not (Figure 4g-j; Figure S3). These results indicate that the tubulin heterodimers released from the internalized axonemes are specifically degraded rather than maintained for reuse. This is consistent with what has been observed for *B. emersonii*, which has high levels of α- and β-tubulin in zoospores that decrease to negligible levels 45 min post-germination when retraction occurs and stay low up to 3 hr post-germination (da Silva & Juliani, 1988).

Tubulin deacetylation via HDAC6 has been associated with cilium disassembly in mammalian cell lines (Ran, Yang, Li, Liu, & Zhou, 2015). That the amount of acetylated tubulin declined at the same rate as α-tubulin suggests that there is no mass deacetylation of tubulin prior to axoneme disassembly or tubulin degradation (Figure 4i,j), although

TABLE 3 Latrunculin A effect on *Spizellomyces punctatus* retraction: parameter quantification

	Control (ethanol)	Latrunculin A
Time to retraction (s)	75.27 ± 47.00	62.33 ± 68.17
Cilium length (μm)	12.26 ± 2.06	12.37 ± 2.02
Rate of retraction (μm/s)	0.26 ± 0.33	0.55 ± 1.04

Note: Using the movies referred to in Figure S2 (ethanol, $n = 81$; latrunculin A, $n = 91$), time to retraction and cilium length were measured in ImageJ and used to calculate rate of retraction for individual cells. The reported rate of retraction is the mean of these individual calculations. Values are shown as mean ± *SD*.

TABLE 4 Latrunculin A effect on *Spizellomyces punctatus* retraction: parameter quantification by retraction type

	Reeling in	Ciliary compartment loss	Lash-around
Control (EtOH) time to retraction (s)	100.55 ± 50.67	44.20 ± 28.27	61.94 ± 23.63
LatA time to retraction (s)	70.83 ± 75.53	58.69 ± 71.22	53.50 ± 52.09
Control (EtOH) cilium length (μm)	12.52 ± 1.95	12.69 ± 2.10	11.15 ± 1.95
LatA cilium length (μm)	12.11 ± 2.18	13.35 ± 1.44	11.66 ± 1.97
Control (EtOH) rate of retraction (μm/s)	0.15 ± 0.08	0.50 ± 0.52	0.20 ± 0.07
LatA rate of retraction (μm/s)	0.34 ± 0.27	0.96 ± 1.77	0.41 ± 0.33
Control (EtOH) retraction events by type (%)	48.1	29.6	22.2
LatA retraction events by type (%)	41.8	30.8	27.5

Note: Using the movies referred to in Figure S2 (ethanol (EtOH) reeling in, $n = 39$; EtOH ciliary compartment loss, $n = 24$; EtOH lash-around, $n = 18$; latrunculin A (LatA) reeling in, $n = 38$; LatA ciliary compartment loss, $n = 28$; LatA lash-around, $n = 25$), time to retraction and cilium length were measured in ImageJ and used to calculate rate of retraction for individual cells. The reported rates of retraction are the means of these individual calculations. "Retraction events by type" indicates the percentage of cells that underwent the indicated retraction type compared with the total number of retraction events for that treatment. Non-percentage values are shown as mean ± *SD*.

our results do not exclude the possibility that tubulin deacetylation and degradation occur in rapid succession.

Possible caveats for this experiment include shed cilium contamination of the sample and new tubulin synthesis during this timecourse. Shear-induced removal of cilia resulted in a reduced α-tubulin band in the cell pellet (Figure S4), indicating that shed cilia do not all end up in protein lysates. Cilia are also only shed ~20% of the time for *R. globosum* and < 5% of the time for *S. punctatus* under normal plating conditions (Figure 4a,b), so we expect shed cilium contamination to be low. Similarly, while we cannot exclude contributions of newly synthesized tubulin during this timecourse, there is no visible internal microtubule network during the phase of the life cycle observed (Figure S1), consistent with a low requirement for tubulin. Additionally, previous work has shown that *B. emersonii* zoospores are transcriptionally and translationally silent, with RNA production starting 40–45 min post-retraction and low levels of protein synthesis beginning 30–40 min later (Lovett, 1968).

2.5 | Axoneme depolymerization and tubulin degradation are partially proteasome dependent

We next tested whether the degradation of internalized axonemal tubulin was dependent on the proteasomal protein degradation pathway. The half-life of tubulin in mammalian cells is about 1 day (Caron, Jones, & Kirschner, 1985; Mooney, Hansen, Langer, Vacanti, & Ingber, 1994), suggesting that an active mechanism is likely required for chytrid axonemal tubulin degradation occurring in hours. The proteasome has also been specifically implicated in cilium disassembly. Ubiquitinated substrates in *Chlamydomonas* increase during cilium disassembly, and *Chlamydomonas* α-tubulin mutants that cannot be ubiquitinated have slower cilium disassembly (Huang, Diener, & Rosenbaum, 2009; Wang, Peng, Long, Deng, & Huang, 2019).

To test the involvement of the proteasome, zoospores of both *R. globosum* and *S. punctatus* were treated with 250 μM of proteasome inhibitor MG132. After 2 hr, MG132-treated cells for both species had more acetylated tubulin remaining than vehicle control cells (Figure 5a–d; Figure S3), although the treatment did not completely protect the tubulin from degradation. This suggests that the internalized axonemal tubulin is degraded at least in part by proteasome-mediated proteolysis. The incomplete penetrance could be due to the involvement of a parallel protein degradation pathway or by only partial inhibition of proteasome activity by MG132 under the conditions used.

We also tested whether axoneme disassembly and tubulin degradation occur concurrently or are separable processes. Zoospores of *R. globosum* and *S. punctatus* were plated with 250 μM MG132 for 10 min, 1 hr, and 2 hr. The percentage of intact internalized axonemes remaining relative to vehicle control cells was quantified by acetylated tubulin immunostaining. For *R. globosum* at 2 hr and *S. punctatus* at 1 hr, cells treated with MG132 had more completely intact axonemes compared to the vehicle control (Figure 5e–f). The percentage increase of intact axonemes was similar to the percentage of total acetylated tubulin remaining in lysates (Figure 5c,d). That blocking tubulin degradation by the proteasome also blocks axoneme depolymerization suggests that the two might be mechanistically linked, with tubulin proteolysis driving disassembly of the complex axoneme structure.

3 | CONCLUSIONS

Cilium disassembly is essential for most ciliated eukaryotic cells to enter the mitotic cycle, but most knowledge about it is limited to a few well-studied organisms. Single-celled eukaryotes have diverse cilium disassembly mechanisms, but little is known about these processes (Bloodgood, 1974). We have shown that two chytrid species, *R. globosum* and *S. punctatus*, rapidly internalize their ciliary axonemes by several mechanisms during cilium disassembly, and we characterized some of the features of this process. Both chytrids disassemble the internalized axonemes and degrade the constituent tubulin over the course of about 2 hr.

Mechanisms for specific types of retraction remain unclear. Lash-around retraction could be mediated by changes in membrane proteins that facilitate membrane fusion; a functionally similar example is agglutinins SAG1 and SAD1 involved in *Chlamydomonas* cilia adhesion during HAP2-dependent gamete fusion (Hernández & Podbilewicz, 2017). Ciliary compartment loss could be caused by disruption of structures at the base of the cilium like the transition zone and distal appendages (Fisch & Dupuis-Williams, 2011). Likely candidates for powering reeling in retraction are the microtubule motor proteins cytoplasmic dynein and kinesins. For example, the rate of retraction of *R. globosum* (0.48 μm/s) is comparable to *in vivo* measurements of speeds of cytoplasmic dynein (1.1 μm/s) and conventional kinesins (1.8 μm/s) (Howard, 1997). There is also precedent for molecular motors being used in the movement of bulky microtubule-based structures like spindles by interactions between microtubules and cortical motors (Carminati & Stearns, 1997; Ellefson & McNally, 2009). Testing these possibilities will require further work on identifying small molecule inhibitors that work in chytrid fungi or developing genetic methods to interfere with function (Medina et al., 2020).

We also hypothesize that there is a relationship between amoeboid motility and the ability to engage in lash-around and ciliary compartment loss retraction. However, chytrid phylogenetic relationships, naming conventions, and methods have drastically changed over time, complicating testing this hypothesis. The most interesting association we found via a cursory attempt to correlate phylogenetic relationships, retraction mechanisms, and amoeboid status is that chytrids concentrated in the Chytridiales, Chytriomyces clade (*R. globosum*, *Chytriomyces hyalinus*, and *Asterophlyctis sarcoptoides*) are non-amoeboid and have no reports of lash-around or ciliary compartment loss retraction (Antikajian, 1949; James, Letcher, et al., 2006; Karling, 1945; Koch, 1968). However, further work will be required to investigate these relationships more completely.

Post-retraction, understanding what factors in the cytoplasm might be interacting with internalized axonemes has implications beyond chytrids. Other circumstances in which the axonemes of

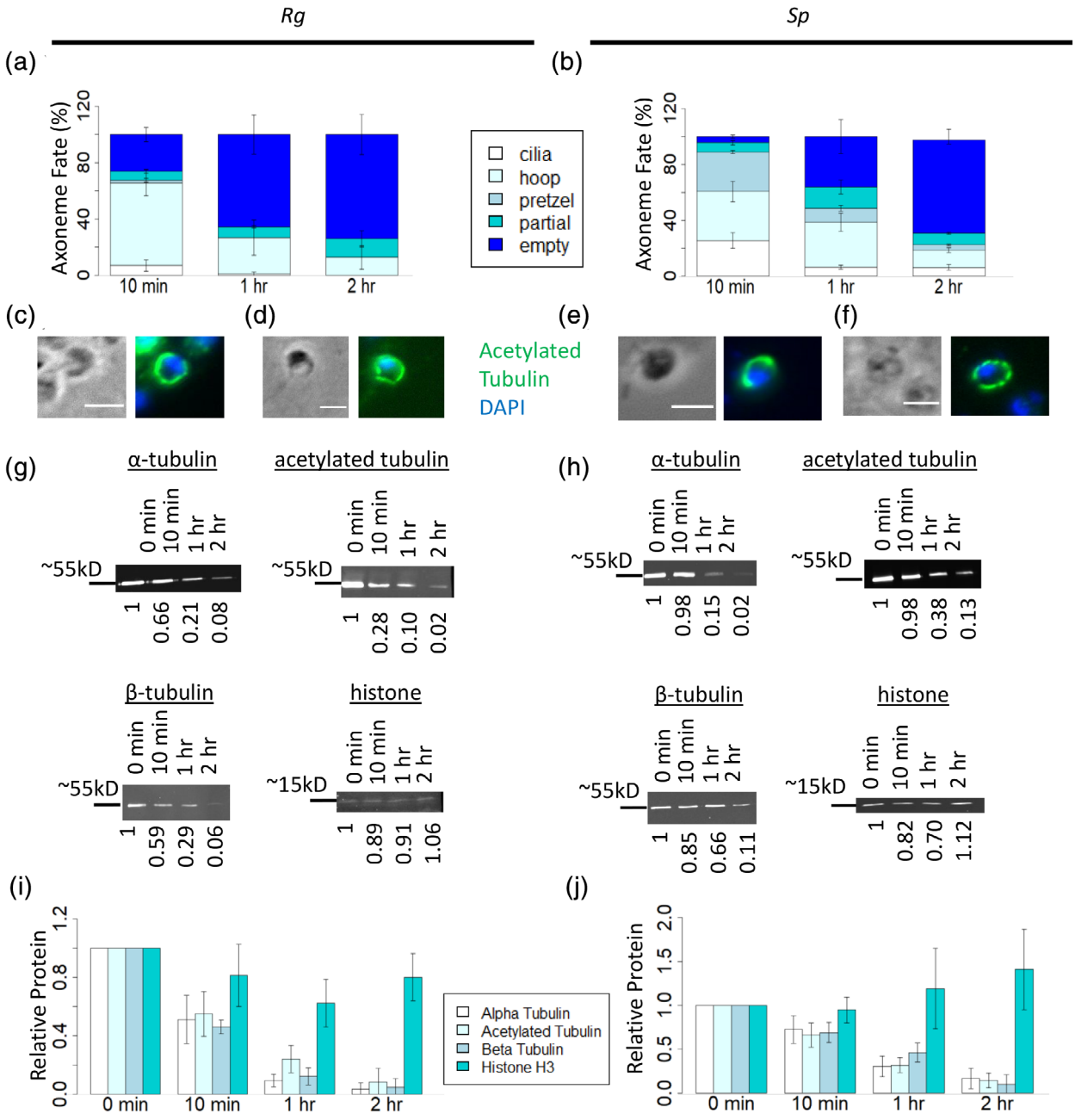

FIGURE 4 Axonemal tubulin is degraded after internalization. Cells were plated for 10 min, 1hr, and 2 hr, fixed, and stained for acetylated tubulin (green) and DNA (blue). Timepoints were quantified for (a) *R. globosum* and (b) *S. punctatus* by the percentage of cells in each of the following categories: cilia, cells that have an exterior cilium; hoop, cells that have a hoop shaped internalized axoneme; pretzel, cells that have an off-cortex internalized axoneme; partial, cells that have one or more fragments of axoneme remaining; and empty, cells that have no axoneme internalized due to axonemal severing or degradation. The quantification reflects four independent experiments for each species. Each timepoint per experiment quantified 47–286 cells for *R. globosum* and 153–408 cells for *S. punctatus*. Examples are shown for *R. globosum* of (c) arcs of axoneme and (d) pieces of axoneme. Examples are also shown for *S. punctatus* of (e) arcs of axoneme and (f) pieces of axoneme. Western blots for α-tubulin, acetylated tubulin, β-tubulin, and histone H3 using lysates for 0 min,10 min, 1 hr, and 2 hr are shown for (g) *R. globosum* and (h) *S. punctatus*. Below each blot is the quantified value for each band normalized to total protein and 0 min. Results were quantified from 3 to 4 independent experiments for each antibody for (i) *R. globosum* and (j) *S. punctatus*. Error bars are *SEM*. Scale bars are 3 μm [Color figure can be viewed at wileyonlinelibrary.com]

motile cilia are in contact with the cytoplasm include animal fertilization in which the sperm axoneme often enters the egg (Bedford, 1972; Simerly et al., 1995) and *Giardia lamblia* which has the proximal portion of its axonemes exposed to cytoplasm (McInally, Kondev, & Dawson, 2019). How programs of dealing with cytoplasm exposed axoneme vary between species throughout the eukaryotic tree remains unknown, and chytrids provide a useful system in which to study this.

Given how important tubulin is to cell function such as the formation of the mitotic spindle and interphase microtubule asters (Nédélec, Surrey, & Karsenti, 2003), it is perhaps surprising that the internalized tubulin is degraded rather than reused during subsequent growth. However, in the early stages of the chytrid life cycle after cilium retraction, we have not observed a significant microtubule cytoskeleton (Figure S1), suggesting that an extensive microtubule network is not needed until later in the life cycle when mitotic divisions begin. With respect to mechanism, we have shown that axonemal tubulin degradation is partially proteasome dependent, but it is unclear whether the remaining degradation activity occurs via a different pathway or if MG132 inhibition of the proteasome in chytrids is incomplete. Another candidate is the autophagy pathway, as blocking autophagy in RPE1 cells blocks cilium disassembly upon serum restimulation (Maharjan et al., 2018).

If not to recycle tubulin for reuse, what is the purpose of internalizing the axoneme? One hypothesis is that degradation of the tubulin provides amino acids for subsequent growth. So far, we have not found any significant difference in the growth rate of cells from which the cilium is sheared off prior to internalization compared to controls on either standard medium or nutritionally poorer minimal medium (Figure S5). Understanding how the decision between cilium retraction and severing is made would have implications for the many single-celled eukaryotic species with multiple possible mechanisms of cilium disassembly.

4 | MATERIALS AND METHODS

Cell Culture: *R. globosum* (JEL800) was grown on PmTG medium (0.1% peptonized milk, 0.1% tryptone, 0.5% glucose) (Barr, 1986). *S. punctatus* (DAOM BR117) was grown on Koch's K1 medium (0.12% peptone, 0.08% yeast extract, 0.24% glucose) (Koch, 1957). The minimal medium used was 0.2X SC pH 7 (0.134% yeast nitrogen base without amino acids and with ammonium sulfate, 0.4% glucose, 0.2% yeast drop-out mix complete, pH to 7.0 with 1 M NaOH). All plates were made with the addition of 1% agar. For zoospore preparation, plates were flooded with medium for a few minutes followed by removal of zoospore-containing medium. Approximately 10^6 cells were plated in 300 μl on 10 cm plates containing solid medium, and the plates were incubated at 23°C. This plating procedure was used for passaging and experiments. The only exception was *S. punctatus* lysate production for histone H3 western blots, where cells from 5 plates at this density were combined for each sample to get sufficient signal. When required, cells were concentrated in a microcentrifuge in two 10 s bursts at 6 k rcf unless otherwise stated. Time zero is defined from when cells were plated unless otherwise stated.

Live-cell imaging: For live imaging of cilium retraction, zoospores were concentrated, resuspended in a smaller volume of medium, and placed between a coverslip and a thin agar pad of the species' appropriate medium or fibronectin-coated hydrogels of 120 kPa stiffness. Imaging occurred on an upright Zeiss Axioskop microscope using a Zeiss 1.3 NA ×40 Ph3 objective or a Zeiss 1.25 NA Ph3 ×63 objective. Videos were captured with phase optics at 30 frames/s using a Sanyo B/W CCD camera digitized with a Canopus ADVC-100. For life cycle imaging, cells were plated on agar plates and imaged every 10 min from zoospore plating to zoospore release. The imaging was done on a Nikon Diaphot with a Nikon 0.25 NA Ph1 ×10 air objective and Hamamatsu Orca-ER digital camera using μManager (Edelstein et al., 2014, https://micro-manager.org/, RRID:SCR_016865).

Immunofluorescence microscopy: Cells were removed from plates with a cell scraper, fixed in 1.5 ml of 4% PFA in PBS, and transferred into a 1.7 ml Eppendorf for 10 min (*R. globosum*) or 1 hr (*S. punctatus*). Cells were concentrated and resuspended in PBS. For *R. globosum*, time points longer than 10 min were treated 1–2 hr with 50 μg/ml chitinase (Sigma-Aldrich, Cat# C6137) in 20 mM potassium phosphate buffer pH 6.0 at 37°C. Cells were spun down onto poly-L-lysine coated coverslips and post-fixed 10 min in −20°C methanol unless phalloidin was used for staining. Coverslips were blocked in PBS-BT (1X PBS, 3% bovine serum albumin, 0.1% Triton-X 100, 0.02% sodium azide) for at least 1 hr and up to overnight. Primary antibody or phalloidin in PBS-BT was added for 2 hr. Concentrations used were: 1:1000 acetylated tubulin 6-11B-1 (Sigma-Aldrich, Cat# T6793, RRID: AB_609894), 1:1000 α-tubulin DM1A (Sigma-Aldrich, Cat# T6199, RRID:AB_477583), and 1:250 14 μM rhodamine-phalloidin (Cytoskeleton, Cat# PHDR1). Secondary antibody with 5 μg/ml DAPI was added for 1 hr before mounting into Mowiol on a slide. Secondary antibodies used 1:1000 in PBS-BT were: Alexa Fluor 488 Goat anti-mouse IgG2b antibody (Thermo Fisher Scientific, Cat# A-21141, RRID:AB_2535778) and Alexa Fluor 647 Goat anti-mouse IgG1 antibody (Thermo Fisher Scientific, Cat#A-21240, RRID:AB_2535809). Cells were imaged on a Zeiss Axiovert 200 M with a Zeiss 1.3 NA Ph3 ×100 oil objective. Exposures were kept constant during experiments, and images were collected using μManager.

Transmission Electron Microscopy: Samples were fixed with 2% glutaraldehyde and 4% paraformaldehyde in 0.1 M sodium cacodylate buffer, pH 7.4 for 1 hr at room temperature. Cells were spun down 2 min at 6 k rpm and resuspended in warm 10% gelatin in PBS for 5 min at 37°C. Samples were placed on ice for 5 min and then spun down for 1 min at 6 k rpm to remove remaining supernatant. Then, 1 ml 1% OsO_4 was added for 2 hr rotating at 4°C. Samples were washed three times for 5 min each at 4°C with water. 1% uranyl acetate in water was added overnight rotating at 4°C. In the morning, samples were dehydrated with a series of 20 min washes of increasing concentrations of ethanol (50% up to 100%). After a final 100% ethanol wash, samples were washed in propylene oxide for 20 min. Samples were then incubated in a 1:1 propylene oxide/Epon solution for 1 hr and a 1:2 propylene oxide/Epon solution overnight. In the morning, samples were transferred to molds with fresh Epon and put in a 65°C polymerization oven. Ultrathin sections were prepared on grids and stained with uranyl acetate and lead citrate just prior to imaging on a JEOL JEM1400 transmission electron microscope.

Lysate Production: Cells were removed from plates with a cell scraper into 1.5 ml of growth media, transferred into a 1.7 ml Eppendorf, and concentrated. Only *S. punctatus* samples were resuspended in 300 μl K1 with protease inhibitors (10 μg/ml PMSF

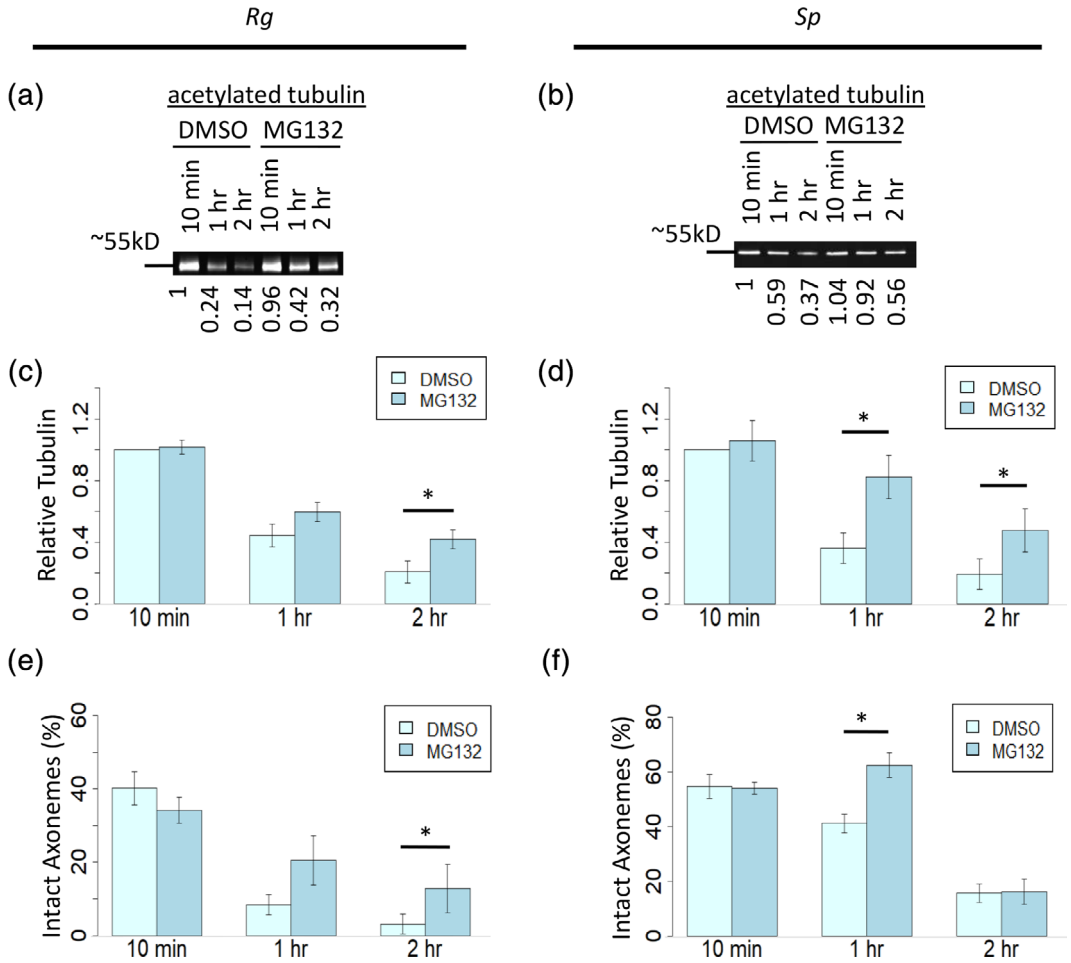

FIGURE 5 Axoneme depolymerization and tubulin degradation are partially proteasome dependent. Lysates were made for cells treated with 250 μM MG132 or 1% DMSO vehicle control for 10 min, 1hr, and 2 hr. Western blots for acetylated tubulin are shown for (a) *R. globosum* and (b) *S. punctatus*. Below each blot is the quantified value for each band normalized to total protein and DMSO 10 min. The results were quantified for (c) *R. globosum* (2 hr $p = .03075$) and (d) *S. punctatus* (1 hr $p = .04013$; 2 hr $p = .03465$) for four independent experiments for each species. Cells were treated with 250 μM MG132 or 1% DMSO for 10 min, 1 hr, and 2 hr, fixed, and stained for acetylated tubulin and DNA. The percentage of completely intact axonemes were quantified for (e) *R. globosum* (2 hr $p = .02813$) and (f) *S. punctatus* (1 hr $p = .02259$). The quantification reflects four independent experiments for *R. globosum* and three for *S. punctatus*. Each condition per experiment quantified 73–444 cells for *R. globosum* and 90–292 cells for *S. punctatus*. Error bars are SEM. * indicates $p < .05$. All other pairs are not significantly different [Color figure can be viewed at wileyonlinelibrary.com]

and 1 mM LPC) for 10 min and concentrated again. After removing the supernatant, 100 μl of reducing and denaturing sample buffer with protease inhibitors was added, and samples were boiled for 10 min at 95°C. For *S. punctatus*, sample buffer was pre-heated to 95°C before use. Cells were transferred on ice to a 0.75 ml Eppendorf with 75 μl of 0.5 mm glass beads. Samples were vortexed for 30 s then left for 30 s on ice five times. A small hole was made in the bottom of the Eppendorf with a 27-gauge needle, and the tube was transferred to nestle inside a 1.5 ml Eppendorf. The sample was spun down 1 min at 16.1 k rcf at 4°C. Samples were boiled another 10 min at 95°C and stored at −20°C.

Cilia Shearing: 10^6 cells in 500 μl medium were pre-incubated with protease inhibitors. Cells were pulled up and down in a syringe 10 times in a 27-gauge needle. Cells were concentrated, and the supernatant was transferred to a new Eppendorf. The pellet was processed into lysates by the above protocol. The supernatant was spun down 10 min at 16.1 k rcf at 4°C before being processed into lysates in the same way.

Western Blots: 30 μl of sample were loaded on 15% acrylamide gel and ran at 120–150 V. Gels were transferred to nitrocellulose membrane, treated with REVERT total protein stain (LICOR, Cat# 926-11011) according to the manufacturer's protocol, and imaged on a LI-COR Odyssey CL-x. Membranes were blocked 30 min in 5% milk in TBST. Membranes were washed three times with TBST, and primary antibody in TBST was added overnight at 4°C except for *S. punctatus* histone H3 blots with the primary added for two nights. Concentrations used are as follows: 1:10,000 α-tubulin DM1A; 1:20,000 acetylated tubulin 6-11B-1; 1:5000 β-tubulin D3U1W (Cell Signaling Technology, Cat# 86298, RRID:AB_2715541); 1:1000 histone H3 EPR17785 (Abcam, Cat# ab201456, RRID:AB_2650560).

The next morning, membranes were washed three times for 5 min in TBST. Secondary antibody was added in TBST. For histone H3, donkey anti-rabbit IgG CW800 (LI-COR, Cat# 926-32213, RRID: AB_621848) was used in a 1:20,000 dilution for 2 hr. For all other primary antibodies, a 1:20,000 dilution of donkey anti-mouse IgG CW800 (LI-COR, Cat# 926–32,212; RRID:AB_621847) was used for 1 hr. Membranes were washed three times for 5 min each in TBST and imaged on a LI-COR Odyssey CL-x.

Small Molecule Inhibitors: For actin inhibition experiments, concentrated zoospores were resuspended in growth media pre-mixed with 0.5% ethanol or 1.2 μM latrunculin A (Cayman Chemical, Cat# 10010630). For proteasome inhibition experiments, concentrated zoospores were resuspended in growth media pre-mixed with 1% DMSO or 250 μM MG132 (Abcam, Cat# ab141003). Following drug introduction, cell lysates and immunofluorescence microscopy samples were prepared as described above starting with plating these cells on non-drugged agar plates. Live cell imaging was also performed as described above starting with placing these resuspended zoospores between a coverslip and thin non-drugged agar pad.

Microscopy Analysis: All live cell imaging and fluorescence microscopy images were processed in ImageJ (https://imagej.nih.gov/ij/; RRID: SCR_003070) or Fiji (https://imagej.net/Fiji; RRID:SCR_002285). Live cell retraction movies were quantified by selecting the frames at the start and end of retraction. Cilium length and cell diameter were measured with the freehand line tool. Live life cycle movies were quantified from their first frame to the frame where the sporangium released its zoospores. For immunofluorescence microscopy timepoints, 20 random fields of view were captured for quantification.

Western Blot Analysis: All western blots were quantified in Fiji using the "Analyze" > "Gels" function. The protein probed for was normalized to the amount of total protein. For untreated cells, these values were then normalized to the first timepoint in the series. For drug-treated cells, these values were normalized to the first timepoint of the vehicle control.

Graph Production and Statistics: Rstudio (https://rstudio.com/; RRID:SCR_000432) was used to produce all graphs and calculate all statistical tests. Box plots report the median as a thick black line, the box as the values between the first and third quartiles, and the extremes as the maximum and minimum values excluding outliers. Individual dots on plots indicate the values from individual cells. Bar graphs report means with error bars as SEM. All reported p values are for Welch's two sample *t* test, an unpaired *t* test. The number of experiments and cells used for each test are reported in the figure legends.

ACKNOWLEDGMENTS

This work was made possible through the National Institutes of Health grant 1R35GM130286 to T.S. This work was also supported by Stanford's NHGRI T32 training grant (project # 5T32HG000044-23) to C.V. TEM was possible through ARRA Award Number 1S10RR026780-01 from the National Center for Research Resources (NCRR). We would like to thank John Perrino and Katie Ching for assistance in TEM image acquisition. We also would like to thank Karen Gonzalez for *S. punctatus* pilot experiments and the Longcore and Buchler labs for providing chytrid species and growth media recipes. Many thanks to members of the Stearns lab for helpful discussion relating to this manuscript.

CONFLICT OF INTEREST

The authors report no conflict of interest.

DATA AVAILABILITY STATEMENT

The data from this work are available from corresponding author Tim Stearns (stearns@stanford.edu) upon request.

ORCID

Claire M Venard https://orcid.org/0000-0003-3660-4976
Tim Stearns https://orcid.org/0000-0002-0671-6582

REFERENCES

Antikajian, G. (1949). A developmental, morphological, and cytological study of *Asterophlyctis* with special reference to its sexuality, taxonomy, and relationships. *American Journal of Botany*, *36*(2), 245–262. https://doi.org/10.1002/j.1537-2197.1949.tb05254.x

Barr, D. J. S. (1986). *Allochytridium expandens* rediscovered: Morphology, physiology and zoospore ultrastructure. *Mycologia*, *78*(3), 439–448. https://doi.org/10.1080/00275514.1986.12025267

Barr, D. J. S., & Hartmann, V. E. (1976). Zoospore ultrastructure of three chytridium species and *Rhizoclosmatium* globosum. *Canadian Journal of Botany*, *54*(17), 2000–2013. https://doi.org/10.1139/b76-214

Bedford, J. M. (1972). An electron microscopic study of sperm penetration into the rabbit egg after natural mating. *American Journal of Anatomy*, *133*(2), 213–254. https://doi.org/10.1002/aja.1001330206

Berger, L., Hyatt, A. D., Speare, R., & Longcore, J. E. (2005). Life cycle stages of the amphibian chytrid *Batrachochytrium dendrobatidis*. *Diseases of Aquatic Organisms*, *68*, 51–63. https://doi.org/10.3354/dao068051

Bloodgood, R. A. (1974). Resorption of organelles containing microtubules. *Cytobios*, *9*(35), 143–161.

Carminati, J. L., & Stearns, T. (1997). Microtubules orient the mitotic spindle in yeast through dynein-dependent interactions with the cell cortex. *Journal of Cell Biology*, *138*(3), 629–641. https://doi.org/10.1083/jcb.138.3.629

Caron, J. M., Jones, A. L., & Kirschner, M. W. (1985). Autoregulation of tubulin synthesis in hepatocytes and fibroblasts. *Journal of Cell Biology*, *101*(5), 1763–1772. https://doi.org/10.1083/jcb.101.5.1763

Chong, J., & Barr, D. J. S. (1973). Zoospore development and fine structures in *Phlyctochytrium* arcticum (Chytridiales). *Canadian Journal of Botany*, *51*(7), 1411–1420. https://doi.org/10.1139/b73-176

da Silva, A. M., & Juliani, M. H. (1988). Regulation of tubulin and actin synthesis and accumulation during *Blastocladiella emersonii* development. *Cell Differentiation*, *24*, 45–54. https://doi.org/10.1016/0045-6039(88)90085-1

Edelstein, A. D., Tsuchida, M. A., Amodaj, N., Pinkard, H., Vale, R. D., & Stuurman, N. (2014). Advanced methods of microscope control using μManager software. *Journal of Biological Methods*, *1*(2), e10. https://doi.org/10.14440/jbm.2014.36

Ellefson, M. L., & McNally, F. J. (2009). Kinesin-1 and cytoplasmic dynein act sequentially to move the meiotic spindle to the oocyte cortex in *Caenorhabditis elegans*. *Molecular Biology of the Cell*, *20*, 2722–2730. https://doi.org/10.1091/mbc.e08-12-1253

Fisch, C., & Dupuis-Williams, P. (2011). Ultrastructure of cilia and flagella – Back to the future! *Biology of the Cell*, *103*, 249–270. https://doi.org/10.1042/BC20100139

Fritz-Laylin, L. K., Lord, S. J., & Mullins, R. D. (2017). WASP and SCAR are evolutionarily conserved in actin-filled pseudopod-based motility. *Journal of Cell Biology*, *216*(6), 1673–1688. https://doi.org/10.1083/jcb.201701074

Fulton, C. (1977). Cell differentiation in *Naegleria gruberi*. *Annual Review of Microbiology*, *31*, 597–629. https://doi.org/10.1146/annurev.mi.31.100177.003121

Hernández, J. M., & Podbilewicz, B. (2017). The hallmarks of cell-cell fusion. *Development*, *144*(24), 4481–4495. https://doi.org/10.1242/dev.155523

Howard, J. (1997). Molecular motors: Structural adaptions to cellular functions. *Nature*, *389*, 561–567. https://doi.org/10.1038/39247

Hu, Z., Liang, Y., He, W., & Pan, J. (2015). Cilia disassembly with two distinct phases of regulation. *Cell Reports*, *10*(11), 1803–1810. https://doi.org/10.1016/j.celrep.2015.02.044

Huang, K., Diener, D. R., & Rosenbaum, J. L. (2009). The ubiquitin conjugation system is involved in the disassembly of cilia and flagella. *Journal of Cell Biology*, *186*(4), 601–613. https://doi.org/10.1083/jcb.200903066

James, T. Y., Kauff, F., Schoch, C. L., Matheny, P. B., Hofstetter, V., Cox, C. J., … Vilgalys, R. (2006). Reconstructing the early evolution of fungi using a six-gene phylogeny. *Nature*, *443*, 818–822. https://doi.org/10.1038/nature05110

James, T. Y., Letcher, P. M., Longcore, J. E., Mozley-Standridge, S. E., Porter, D., Powell, M. J., … Vilgalys, R. (2006). A molecular phylogeny of the flagellated fungi (*Chytridiomycota*) and description of a new phylum (*Blastocladiomycota*). *Mycologia*, *98*(6), 860–871. https://doi.org/10.1080/15572536.2006.11832616

James, T. Y., Toledo, L. F., Rödder, D., da Silva Leite, D., Belasen, A. M., Betancourt-Román, C. M., … Longcore, J. E. (2015). Disentangling host, pathogen, and environmental determinants of a recently emerged wildlife disease: Lessons from the first 15 years of amphibian chytridiomycosis research. *Ecology and Evolution*, *5*(18), 4079–4097. https://doi.org/10.1002/ece3.1672

Karling, J. S. (1945). Brazilian chytrids. VI. Rhopalophlyctis and Chytriomyces, two new chitinophyllic operculate genera. *American Journal of Botany*, *32*(7), 362–369. https://doi.org/10.2307/2437353

Kim, S., Lee, K., Choi, J.-H., Ringstad, N., & Dynlacht, B. D. (2015). Nek2 activation of Kif24 ensures cilium disassembly during the cell cycle. *Nature Communications*, *6*, 8087. https://doi.org/10.1038/ncomms9087

Koch, W. J. (1957). Two new chytrids in pure culture, *Phlyctochytrium* punctatum and *Phylctochytrium* irregulare. *Journal of the Elisha Mitchell Scientific Society*, *73*(1), 108–122.

Koch, W. J. (1968). Studies of the motile cells of chytrids V. Flagellar retraction in posteriorly uniflagellate fungi. *American Journal of Botany*, *55*(7), 841–859. https://doi.org/10.1002/j.1537-2197.1968.tb07442.x

Laundon, D., Chrismas, N., Wheeler, G., & Cunliffe, M. (2020). Chytrid rhizoid morphogenesis resembles hyphal development in multicellular fungi and is adaptive to resource availability. *Proceedings of the Royal Society B*, *287*(1928), 20200433. https://doi.org/10.1098/rspb.2020.0433

Leshem, T., Letcher, P. M., Powell, M. J., & Sukenik, A. (2016). Characterization of a new chytrid species parasitic on the dinoflagellate, *Peridinium gatunense*. *Mycologia*, *108*(4), 731–743. https://doi.org/10.3852/15-197

Letcher, P. M., Longcore, J. E., Quandt, C. A., Leite, D. d. S., James, T. Y., & Powell, M. J. (2017). Morphological, molecular, and ultrastructural characterization of *Rozella rhizoclosmatii*, a new species in Cryptomycota. *Fungal Biology*, *121*(1), 1–10. https://doi.org/10.1016/j.funbio.2016.08.008

Liang, Y., Meng, D., Zhu, B., & Pan, J. (2016). Mechanism of ciliary disassembly. *Cellular and Molecular Life Sciences*, *73*, 1787–1802. https://doi.org/10.1007/s00018-016-2148-7

Linck, R. W., Chemes, H., & Albertini, D. F. (2016). The axoneme: The propulsive engine of spermatozoa and cilia and associated ciliopathies leading to infertility. *Journal of Assisted Reproduction and Genetics*, *33*(2), 141–156. https://doi.org/10.1007/s10815-016-0652-1

Lohret, T. A., McNally, F. J., & Quarmby, L. M. (1998). A role for katanin-mediated axonemal severing during *Chlamydomonas* deflagellation. *Molecular Biology of the Cell*, *9*(5), 1195–1207. https://doi.org/10.1091/mbc.9.5.1195

Longcore, J. E., Pessier, A. P., & Nichols, D. K. (1999). *Batrachochytrium dendrobatidis* gen. et sp. nov., a chytrid pathogenic to amphibians. *Mycologia*, *91*(2), 219–227. https://doi.org/10.1080/00275514.1999.12061011

Lovett, J. S. (1968). Reactivation of ribonucleic acid and protein synthesis during germination of *Blastocladiella* zoospores and the role of the ribosomal nuclear cap. *Journal of Bacteriology*, *96*(4), 962–969. https://doi.org/10.1128/jb.96.4.962-969.1968

Maharjan, Y., Lee, J. N., Kwak, S. A., Lim, H., Dutta, R. K., Liu, Z., … Park, R. (2018). Autophagy alteration prevents primary cilium disassembly in RPE1 cells. *Biochemical and Biophysical Research Communications*, *500*(2), 242–248. https://doi.org/10.1016/j.bbrc.2018.04.051

McInally, S., Kondev, J., & Dawson, S. (2019). Length-dependent disassembly maintains four different flagellar lengths in *giardia*. *eLife*, *8*, e48694. https://doi.org/10.7554/eLife.48694

Medina, E. M., Robinson, K. A., Bellingham-Johnstun, K., Ianiri, G., Laplante, C., Fritz-Laylin, L. K., & Buchler, N. E. (2020). Genetic transformation of *Spizellomyces punctatus*, a resource for studying chytrid biology and evolutionary cell biology. *eLife*, *9*, e52741. https://doi.org/10.7554/eLife.52741

Mirvis, M., Siemers, K. A., Nelson, W. J., & Stearns, T. P. (2019). Primary cilium loss in mammalian cells occurs predominantly by whole-cilium shedding. *PLoS Biology*, *17*(7), e3000381. https://doi.org/10.1371/journal.pbio.3000381

Miyamoto, T., Hosoba, K., Ochiai, H., Royba, E., Izumi, H., Sakuma, T., … Matsuura, S. (2015). The microtubule-depolymerizing activity of a mitotic kinesin protein KIF2A drives primary cilia disassembly coupled with cell proliferation. *Cell Reports*, *10*(5), 664–673. https://doi.org/10.1016/j.celrep.2015.01.003

Mooney, D. J., Hansen, L. K., Langer, R., Vacanti, J. P., & Ingber, D. E. (1994). Extracellular matrix controls tubulin monomer levels in hepatocytes by regulating protein turnover. *Molecular Biology of the Cell*, *5*(12), 1281–1288. https://doi.org/10.1091/mbc.5.12.1281

Nédélec, F., Surrey, T., & Karsenti, E. (2003). Self-organisation and forces in the microtubule cytoskeleton. *Current Opinion in Cell Biology*, *15*(1), 118–124. https://doi.org/10.1016/s0955-0674(02)00014-5

Parker, J. D. K., Hilton, L. K., Diener, D. R., Rasi, M. Q., Mahjoub, M. R., Rosenbaum, J. L., & Quarmby, L. M. (2010). Centrioles are freed from cilia by severing prior to mitosis. *Cytoskeleton*, *67*(7), 425–430. https://doi.org/10.1002/cm.20454

Pessier, A. P., Nichols, D. K., Longcore, J. E., & Fuller, M. S. (1999). Cutaneous chytridiomycosis in poison dart frogs (Dendrobates spp.) and White's tree frogs (*Litoria caerulea*). *Journal of Veterinary Diagnostic Investigation*, *11*(2), 194–199. https://doi.org/10.1177/104063879901100219

Piao, T., Luo, M., Wang, L., Guo, Y., Li, D., Li, P., … Pan, J. (2009). A microtubule depolymerizing kinesin functions during both flagellar disassembly and flagellar assembly in *Chlamydomonas*. *PNAS*, *106*(12), 4713–4718. https://doi.org/10.1073/pnas.0808671106

Ran, J., Yang, Y., Li, D., Liu, M., & Zhou, J. (2015). Deacetylation of alpha-tubulin and cortactin is required for HDAC6 to trigger ciliary disassembly. *Scientific Reports*, *5*, 12917. https://doi.org/10.1038/srep12917

Simerly, C., Wu, G.-J., Zoran, S., Ord, T., Rawlins, R., Jones, J., … Schatten, G. (1995). The paternal inheritance of the centrosome, the

cell's microtubule-organizing center, in humans, and the implications for infertility. *Nature Medicine*, *1*(1), 47–52. https://doi.org/10.1038/nm0195-47

Sparrow, F. K. (1960). *Aquatic Phycomycetes (2nd ed.)*, Ann Arbor, MI: . The University of Michigan Press.

Truesdell, L. C., & Cantino, E. C. (1971). The induction and early events of germination in the zoospore of *Blastocladiella emersonii*. *Current Topics in Developmental Biology*, *6*(6), 1–44. https://doi.org/10.1016/S0070-2153(08)60636-5

Vélez, C. G., Letcher, P. M., Schultz, S., Powell, M. J., & Churchill, P. F. (2011). Molecular phylogenetic and zoospore ultrastructural analyses of *Chytridium olla* establish the limits of a monophyletic Chytridiales. *Mycologia*, *103*(1), 118–130. https://doi.org/10.3852/10-001

Wang, Q., Peng, Z., Long, H., Deng, X., & Huang, K. (2019). Poly-ubiquitylation of alpha-tubulin at K304 is required for flagellar disassembly in *Chlamydomonas*. *Journal of Cell Science*, *132*(6), jcs229047. https://doi.org/10.1242/jcs.229047

SUPPORTING INFORMATION

Additional supporting information may be found online in the Supporting Information section at the end of this article.

How to cite this article: Venard CM, Vasudevan KK, Stearns T. Cilium axoneme internalization and degradation in chytrid fungi. *Cytoskeleton*. 2020;77:365–378. https://doi.org/10.1002/cm.21637